We are IntechOpen, the world's leading publisher of Open Access books Built by scientists, for scientists

6,900
Open access books available

185,000
International authors and editors

200M
Downloads

154
Countries delivered to

Our authors are among the

TOP 1%
most cited scientists

12.2%
Contributors from top 500 universities

CLARIVATE ANALYTICS
BOOK CITATION INDEX
INDEXED

WEB OF SCIENCE™

Selection of our books indexed in the Book Citation Index
in Web of Science™ Core Collection (BKCI)

Interested in publishing with us?
Contact book.department@intechopen.com

Numbers displayed above are based on latest data collected.
For more information visit www.intechopen.com

Chapter

The Investigation of the Dorfak Karstic Aquifer

Maryam Dehban Avan Stakhri, Mohammad Hossien Ghobadi and Ali Mirarabi

Abstract

The karstic aquifers were the best source of potable water in the northeast of Rudbar, Iran. The present study was carried out to appraise the hydrogeological attributes of karst aquifer in this area. For this objective, saturation indices (SI values) are acquired through using the geochemical PHREEQC software for a number of chemical compounds existing in the karstic aquifer. Moreover, the sources of the ions and hydrogeochemical plots were obtained by using AqQA-RockWare software packages. The water type of all springs is the Ca-HCO$_3$ type which is determined by plotting of Piper diagram and Durov diagram for spring water samples, that is confirming the calcareous effects of the region on the quality of groundwater and representing a single source for the springs. The degree of Karstification of the recharge area of the karst aquifer was determined to be 5.5 from an analysis of the hydrograph Sefidab Spring. The microbial contamination can be observed in all samples due to the intense development of karst, lack of self-purification in the karst system, and lack of an adequate cover layer on carbonate formation.

Keywords: Dorfak, saturation indices, chloro-alkaline index, cross diagram, recession curve

1. Introduction

Iran as a dry country with a population of 80 million has faced a water deficit in recent decades. The unorganized use of groundwater resources is created by subsidence of many plains in Iran. Guilan, a province situated in the north of Iran, has wet weather and thus is less subjected to water shortage problems compared to the southern and central provinces of Iran. The Dorfak karstic area is situated in the northeast part of the Rudbar city (**Figure 1**). The highest point of the area is a Dorfak peak with a height of 2733 m.a.s.l (meters above sea level). The karstic aquifers (excluding of the evaporating formation) are suitable groundwater resources for potable water. Dorfak karstic area is the initial well-known karstic region of Guilan province. The first study in this area was conducted by the Water Resources Management Company of Iran. In the following, we investigate the study area in terms of geology, tectonic structures, climate, and quantitative and qualitative properties of the aquifer by the analysis of water samples from springs in the region. For this purpose, information about the discharge rates of these springs and their chemical analysis was provided by the Regional Water Company of Guilan province. Information about various lithologies in the region was obtained

Figure 1.
Situation map of the study area [1].

using the 1:100,000-scale geological map published by Geological Survey of Iran. Additionally, a hydrograph analysis method was also used to estimate the degree of karstification in recharge areas.

2. Topography, climate, and vegetation

The Dorfak karst area, one of the largest karst regions of the north-east of Rudbar city, is situated in the east of the Guilan province of Iran. The region area ranges from about 1000 m elevation up to the Dorfak summit at 2733 m.a.s.l. The whole mountain range covers an area of about 429.59 km². The study area is affected by two climates: Csa and Bsk. The majority of the study area is situated in the Csa climate. The monthly average minimum and maximum temperature is 0.40°C in February and 18.5°C in August. The mean annual rainfall has been

748 mm in the last 20 years (1993–2013). The most rainfall occurs in November, December, March, and February, in the order of their appearance. The Csa Mediterranean climate can be observed in the western continents between latitude 30–45°. The rainy weather and hot and dry summers are special characteristics of this climate. The climate depends on the high-pressure semitropic system, except that coastal areas have a cooler summer because of the cold ocean flow. This cool ocean flow often creates fog and prevents rainfall. Up to an elevation of approximately 2000 m, vegetation is covered by forests with beech trees in the west and north-west parts. Above the timberline, grassy vegetation persists up to the summit, where soil coverage has not been washed out due to karstification or erosion.

3. Stratigraphy and tectonic structures

The Dorfak karst area is a part of the West Alborz that is situated on the east of the Sefidrud Valley. The trend of the mountains was east-west (EW). In the southern slope of the Dorfak summit, one can observe the outcrop of the volcanic
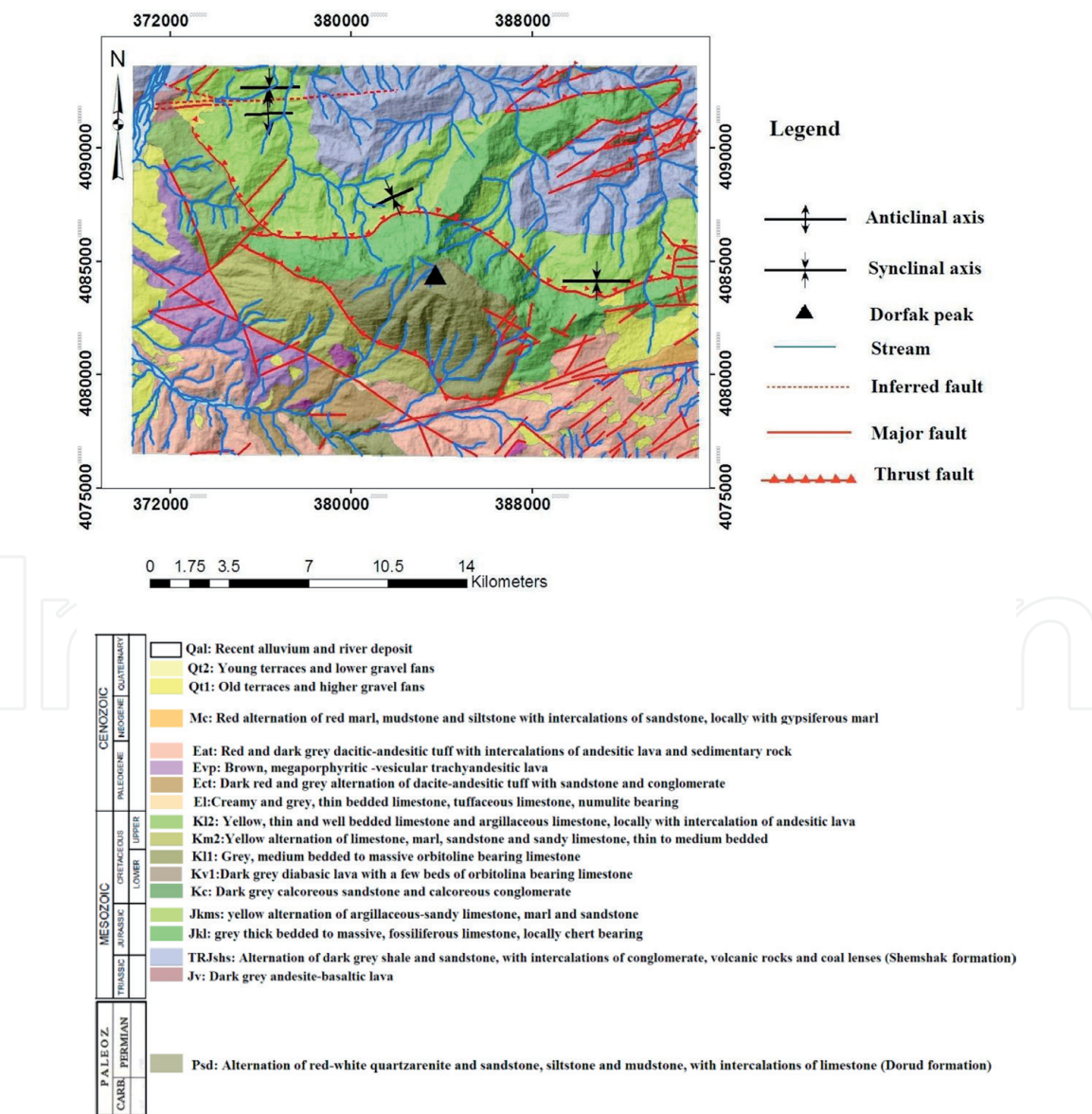

Figure 2.
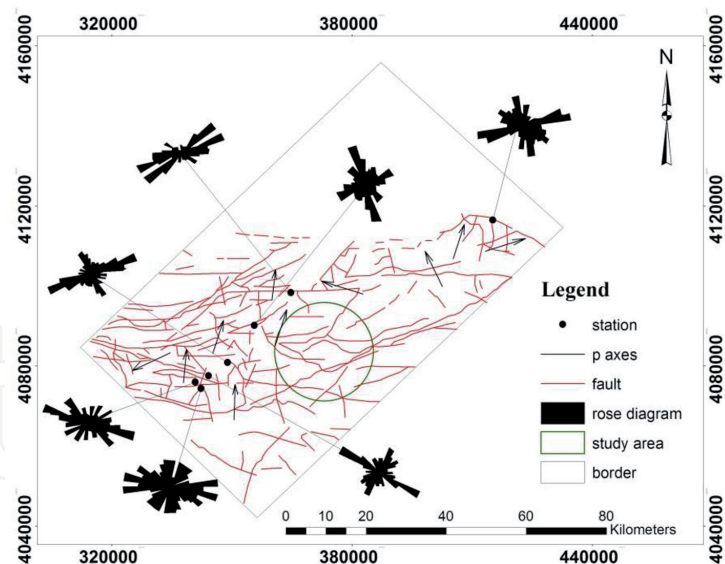*Geology map of the study area [1].*

Figure 3.
Structure geology map of the study area (reproduced with the permission from [2]).

rocks with the Paleogene age. The limestone units in the Dorfak karstic area contain gray thick to massive bedded fossiliferous limestone, which is locally chert-bearing (JKL), gray, medium-bedded limestone including Orbitolina fossils (KL1); alternating beds of yellow argillaceous-sandy limestone, marl and sandstone (JKms); alternating beds of thin- to medium-bedded limestone, marl, sandstone and sandy limestone (Km2); and thin and well-bedded limestone and argillaceous limestone, locally with intercalation of andesitic lava (KL2) (**Figure 2**) [1]. The effects of the Arabian Plate's pressure on the Eurasian Plate can be observed in the reported kinetic axes for the West Alborz that is directed from the northeast to the north. In the view of structural geology, the Dorfak karstic area was situated in Lahijan fault shear zone. Safari et al. [2] were reported that the main compression axis for the Lahijan shear zone is N10E. This result is confirmed due to the former measured pressure axis in the area and left-lateral movement of Lahijan fault. The pop-up structure of the Dorfak peak was created by the enclosure between two thrust faults, which are the Dorfak thrust fault with a slope to the south and the Deylaman thrust fault with a slope to the north (**Figure 3**). This structure provides a sui basis for the karst development through creating of the large fractures in rocks of the area [1]. The trend of these faults was almost perpendicular to in this region. The strike of faults was N90s–110 and has reverse movement with a left-lateral component [2].

4. Karst features

One of the main properties of karstification is the existence of karst features. In order to determine the karst extent in the study area, karst features were identified. The critical features of karstic regions such as the presence of sinkholes, karrens, shafts, caves, poljes, and springs can be observed in the Dorfak karst area. The different types of karrens such as grikes, clints, kamenitzas, rinnenkarren, meandering runnels, wall karren, hummocky karren, trittkarren, rainpits, rillenkarren, rundkarren, and cavernous karren are observed in the study area. Sinkholes are prevailing features in the karst region. The types of sinkholes are solution and collapsible. Shafts are prevailing features due to the high abundance of joints with an upright dip in the Dorfak peak. The Dorfak bowl is a polje that its water is supplied through melting snow and drainage of rainfall into the polje. **Figure 4** shows some karst features.
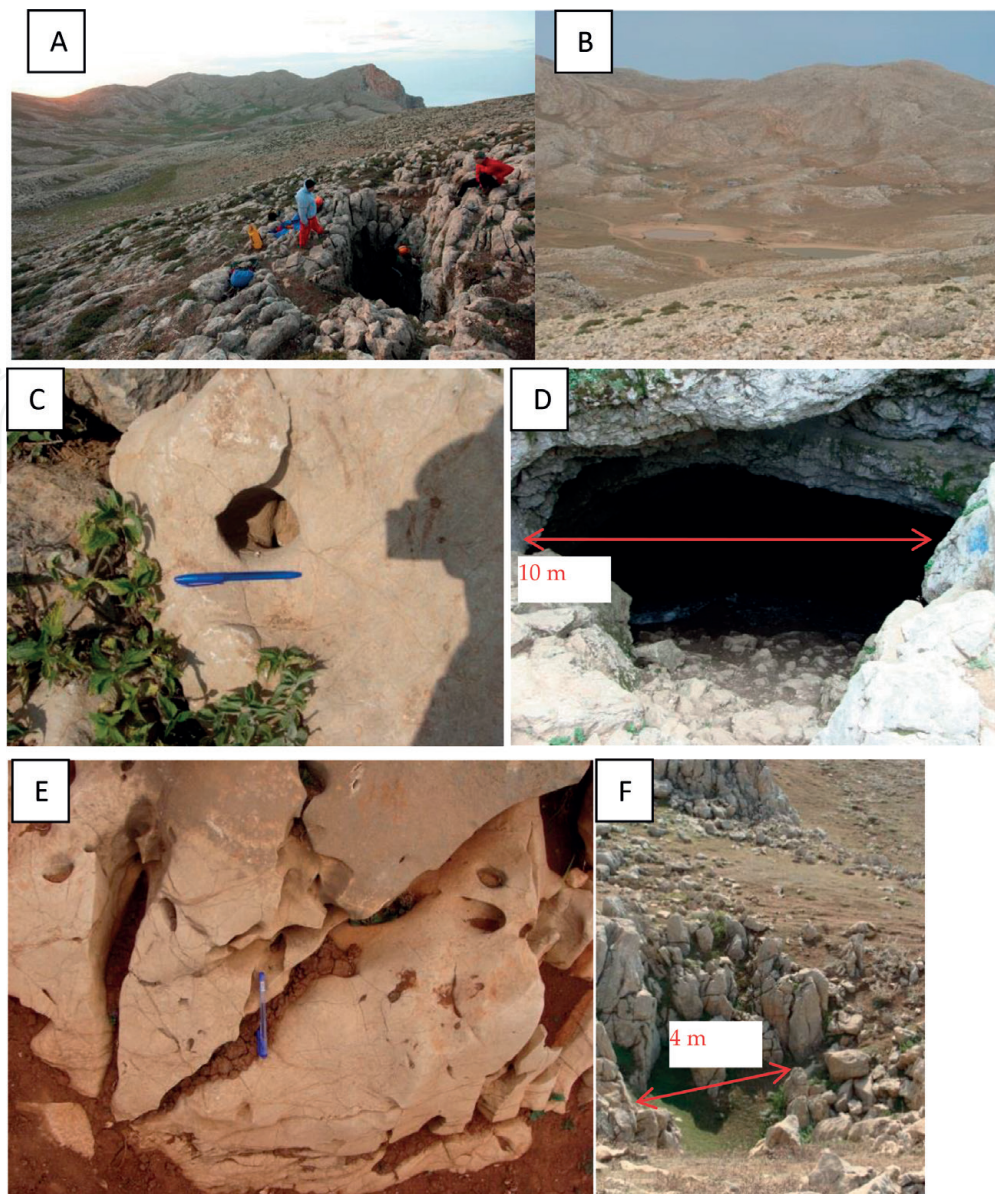
Figure 4.
Images of some karst features in the study area (Dorfak peak), A: a shaft (Afraz scaler group of Rasht city), B: polje, C: Kamenica, D: Dorfak cave, E: Rundkarren, and F: sinkhole.

5. Hydrogeology of the spring

There are several springs in the Dorfak karstic area. The spring's situation is shown in **Figure 5**. In this section, we will investigate Sefidab spring properties as the most important spring of the Dorfak karst area. Sefidab spring operates as the permanent drain of the Dorfak karst aquifer. The Sefidab spring is situated in the west side of the Dorfak peak, in the Sefidab valley, 387 m.a.s.l (**Figure 6**). The annual average discharge of Sefidab spring is 500 l/s that the watershed area of spring was inappreciable against discharge content and it is about 2 km^2. The runoff content of Kharashk watershed is considerably higher than the total content of precipitation because of the high development of karst in this subbasin; the water transition through shafts and sinkholes is situated in the upstream subbasin. The Sefidab spring is a typical fault-bound and limestone karst spring with a dynamic outflow. Since exact measurements done in June 2011, the highest discharge was recorded on December 21, 2013, with more than 2534 l/s. The lowest discharge was recorded on July 14, 2012 with 30 l/s. The mean discharge in this period (2011–2014) reached 500 l/s. The present study investigates the hydrogeochemical attributes of
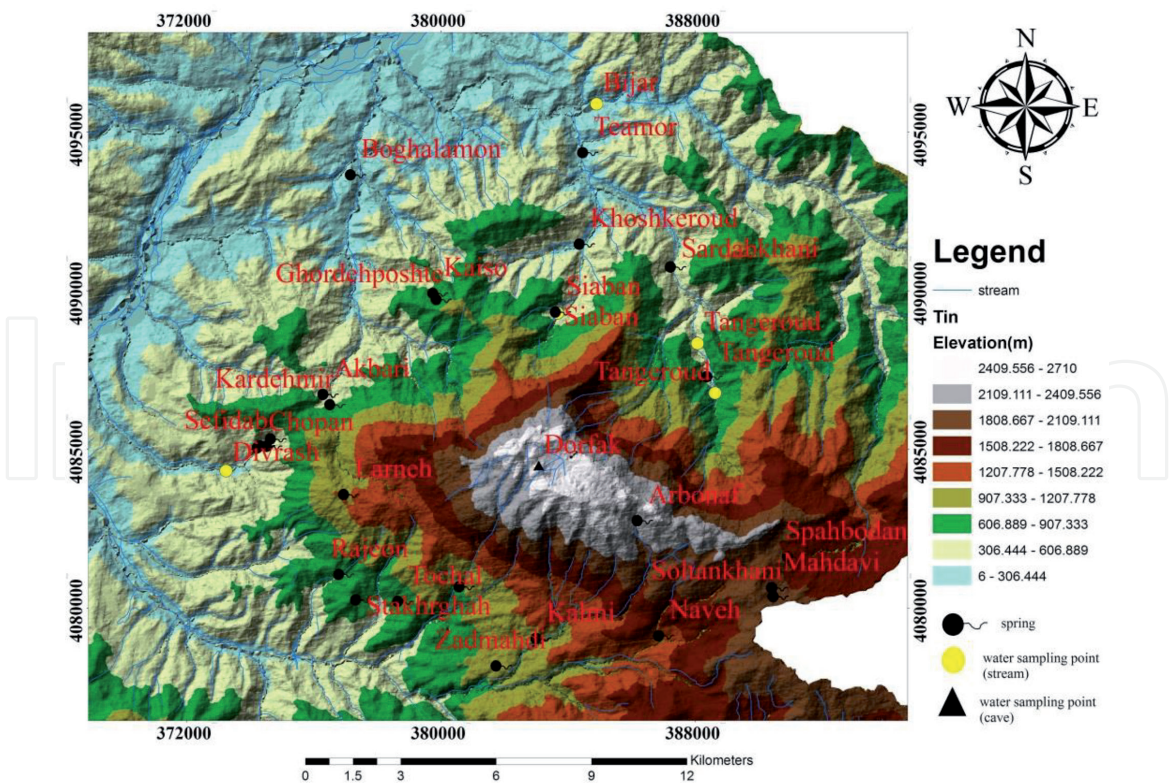
Figure 5.
Situation map of springs and sample point in the study area.

Figure 6.
Images of the Sefidab spring in the study area.

the karst aquifer through the analysis of water samples from karst springs in the area. For achieving this goal, database of the Regional Water Company of Guilan province about the discharge rates of these springs and their chemical analysis was used. Information about various lithologies in the region was obtained using the 1:100,000-scale geological map published by Geological Survey of Iran. A hydrograph analysis method was also used to estimate the degree of karstification in recharge areas.

6. Geochemistry investigation

By plotting a Piper diagram [3] of spring water samples, the water type of all sources of the region was discovered to be the Ca-HCO3 type, demonstrating that all springs in the region were discharged from a karst aquifer (**Figure 7**). Plotting of the Durov diagram of the samples is done to attain an accurate inspection of the chemical attributes of groundwater (**Figure 8**). Compared to Piper diagram, the Durov diagram distinguishes in terms of its ability to showing different types of water and hydrochemical processes such as water mixing of different qualities and ion exchange [4]. The chemical composition of springs is bicarbonate type with the Ca cation being the dominant by using the Durov diagram, which has also confirmed the effects of limestone formations on the quality of groundwater in the region. Also, using the Durov diagram has proven that the springs recharge usually from a single origin. The anionic evolution cycle has more effect on the ion evolutionary cycle of groundwater than the cationic cycle, which has been obviously proven due to the increasing total dissolved solids (TDS) in water sample of springs. The groundwaters of the area are situated into the domain of alkaline springs due to the plotting of the Durov diagram. The statistical parameters of chemical analysis results of elective resource can be observed in **Tables 1** and **2**.
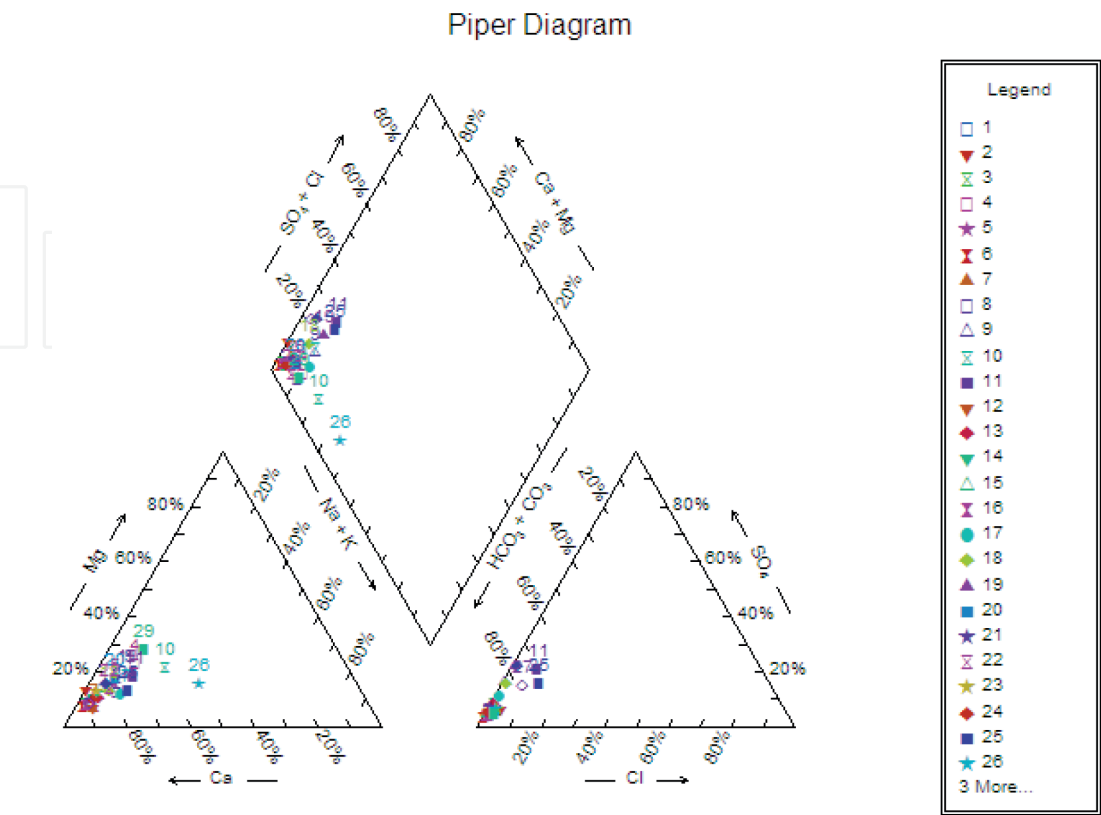

Figure 7.
Piper diagram of water sample.

A Cl-HCO$_3$-SO$_4$ ternary diagram (**Figure 9**) showed distinct zones of alkaline, acidic, and chloride-rich water [6]. As shown in **Figure 9**, all water samples are located in the soda spring zone.

In order to evaluate the controlling mechanisms of water chemistry, the effect of host rock lithology on water quality is estimated, and the mechanism of groundwater flow is determined, and the composition of the main ions in groundwater is applied as per the Gibbs chart (1970) [7]. The effective mechanisms of water chemistry and its evolution are separated into three classes by Gibbs: atmospheric precipitation, rock weathering, and evaporation [8]. Also, he proposed two diagrams of $Na^+/(Na^+ + Ca^{2+})$ and $Cl^-/(Cl^- + HCo_3^-)$ against the TDS to appraise the origin of dissolved chemical constituents in water.
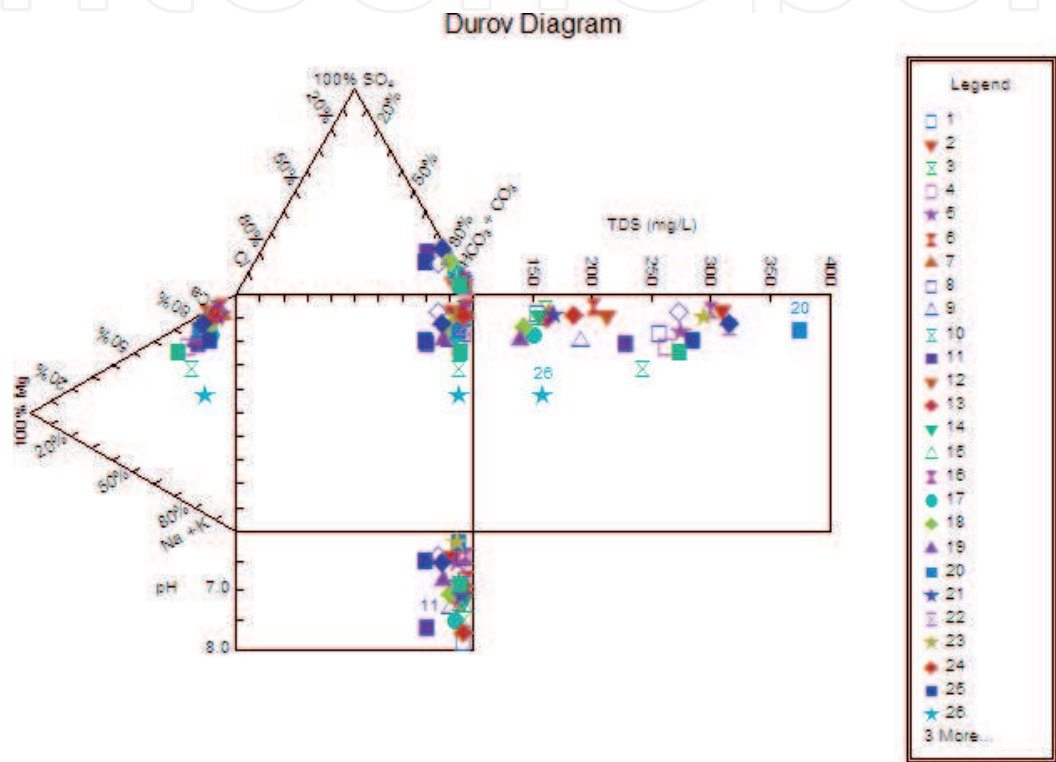

Figure 8.
Durov diagram of water samples.

Dry season												
Parameters	**Ec (µs/cm)**	**TDS (mg/l)**	**pH**	**meq/l**								
				HCO$_3^-$	**CO$_3^-$**	**Cl$^-$**	**SO$_4^-$**	**NO$_3^-$**	**Ca$^+$**	**Mg^{2+}**	**Na$^+$**	**K$^+$**
Number of samples	29	29	29	29	29	29	29	29	29	29	29	29
Average	354.34	222.7	6.99	3.48	0	0.07	0.22	0.09	3.08	0.54	0.29	0.04
Maximum	630	375.8	7.9	6.15	0	0.33	0.75	0.61	5	1.37	0.94	0.18
Minimum	159	140.06	6.2	1.94	0	0.01	0.09	0.01	1.38	0.17	0.06	0.01
Standard deviation	124.78	65.52	0.46	1.13	0	0.08	0.15	0.12	1.02	0.32	0.22	0.04
Variation coefficient	0.35	0.3	0.65	0.32	0	1.14	0.68	1.33	0.33	0.59	0.75	1

Table 1.
Statistics parameters of chemical analysis results of elective resource in the dry season [5].

Wet season												
Parameters	Ec (μs/cm)	TDS (mg/l)	pH	meq/l								
				HCO_3^-	CO_3^-	Cl^-	SO_4^-	NO_3^-	Ca^+	Mg^{2+}	Na^+	K^+
Number of samples	30	30	30	30	30	30	30	30	30	30	30	30
Average	334.81	203.28	7.48	3.09	0	0.11	0.18	0.13	2.86	0.47	0.25	0.02
Maximum	595	355.65	8.55	5.96	0	0.72	0.61	1.39	4.83	1.12	2.41	0.1
Minimum	69.7	44.35	6.88	0.6	0	0.03	0.07	0.005	0.4	0.17	0.03	0
Standard deviation	140.51	83.26	0.42	1.32	0	0.13	0.1	0.25	1.28	0.25	0.43	0.02
Variation coefficient	0.42	0.41	0.05	0.43	0	1.19	0.56	1.92	0.45	0.53	1.72	1

Table 2.
Statistics parameters of chemical analysis results of elective resource in the wet season [5].
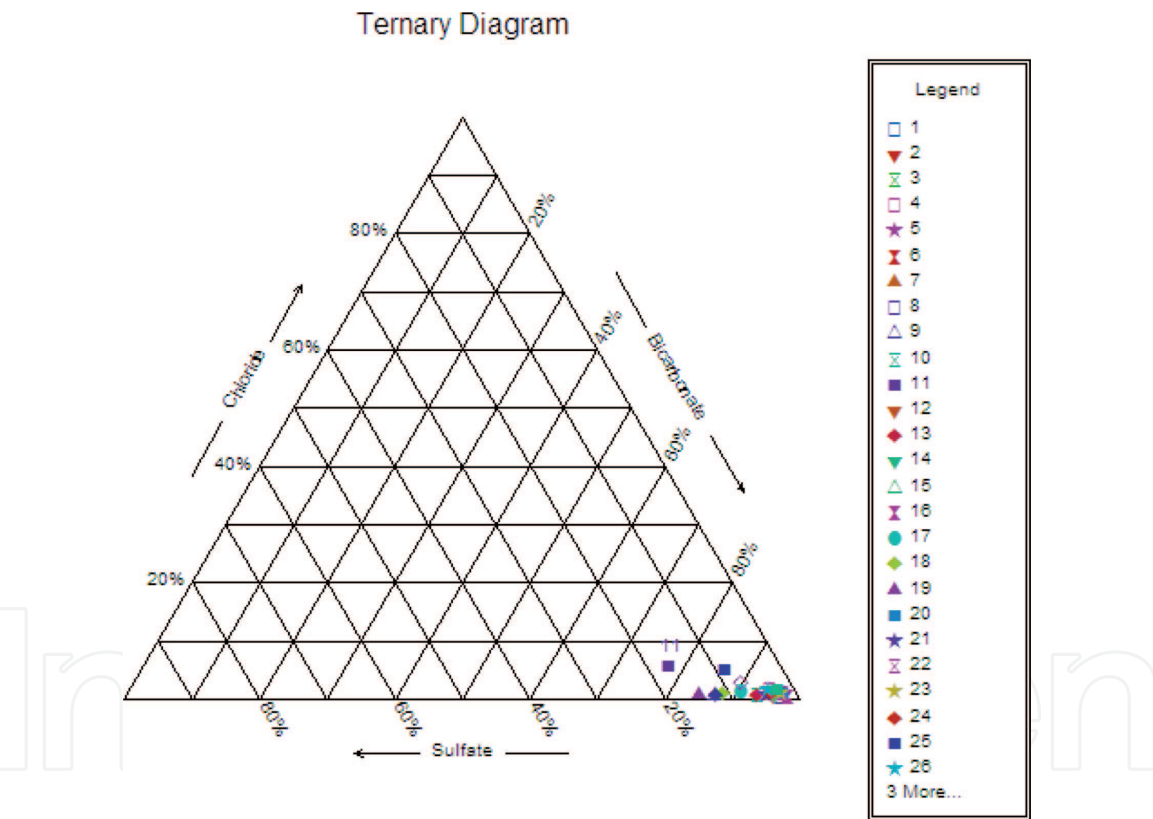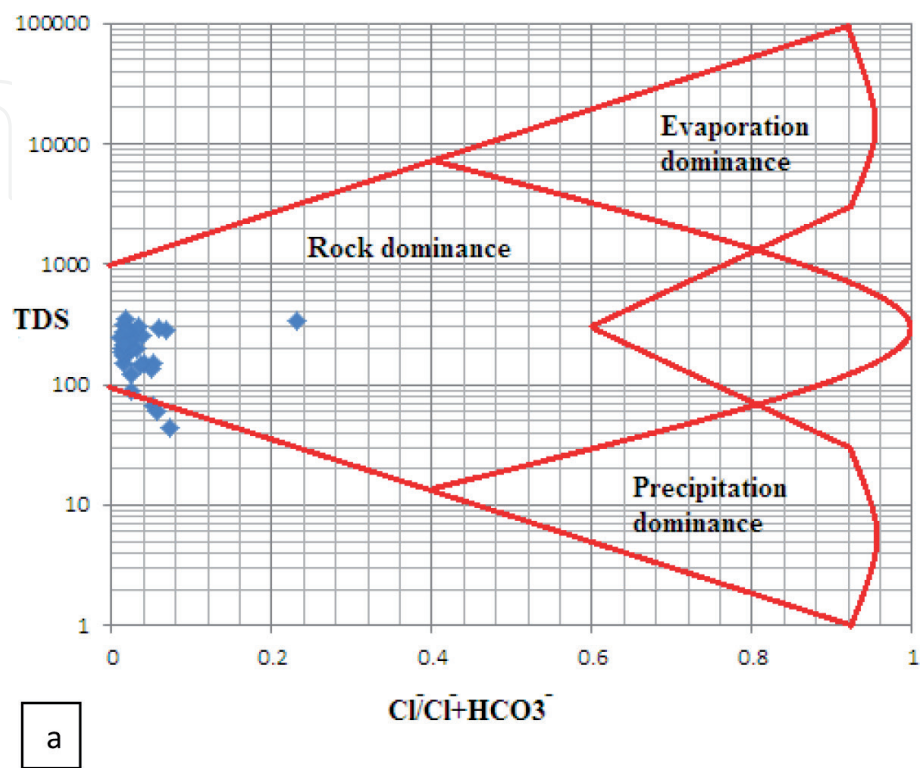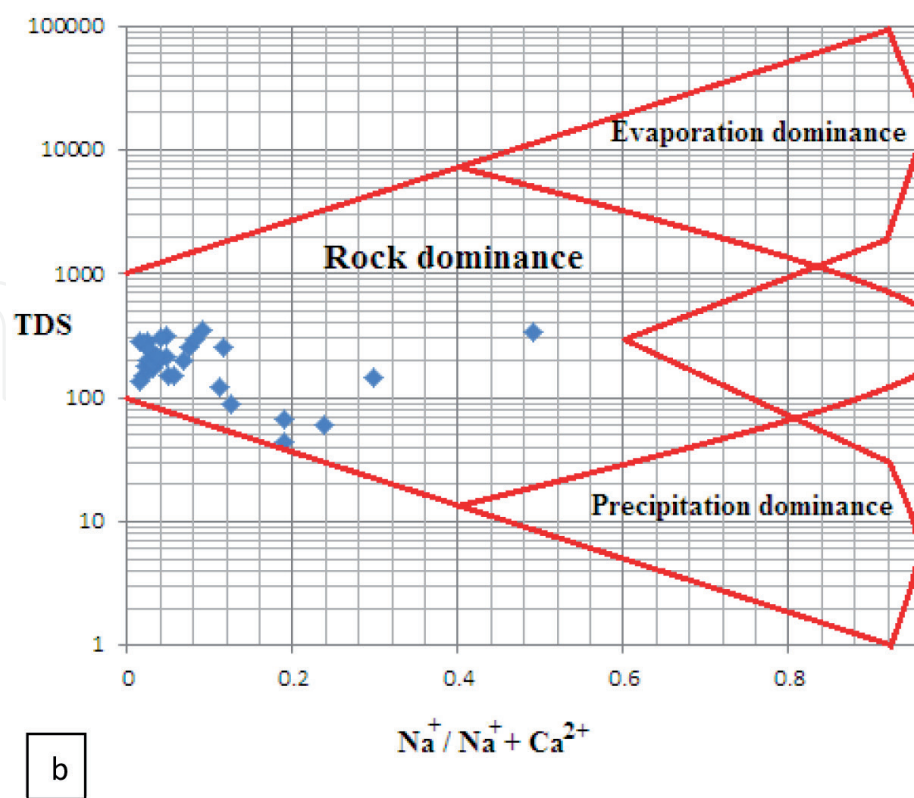

Figure 9.
Ternary diagram (Cl-HCO₃-SO₄) of the water samples.

In samples with a high ratio of $Na^+/(Na^+ + Ca^{2+})$ or $Cl^-/(Cl^- + HCO_3^-)$ and low amount of TDS, salts derived from rainfall are likely to have a significant effect on the chemistry of water in the study area. In contrast, in samples with a low ratio of $Na^+/(Na^+ + Ca^{2+})$ or $Cl^-/(Cl^- + HCO_3^-)$ and TDS between 100 and 1000 mg/L, rock weathering is likely to affect the groundwater quality. Finally, samples with a higher salinity are likely to be affected by evapotranspiration. Extensive changes in the ratio of $Na^+/(Na^+ + Ca^{2+})$ or $Cl^-/(Cl^- + HCO_3^-)$ with an almost constant TDS probably show that ion exchange affects groundwater quality in the region [1]. During an ion exchange process, 1 mmol/L of calcium was substituted with 2 mmol/L of

sodium, which cannot significantly change the amount of TDS in the water, because the weight of 1 mmol/L of calcium (40 mg/L) was almost two times of 2 mmol/L of sodium (46 = 2 × 23 mg/L) [9]. According to these diagrams (**Figure 10a** and **b**), the water samples were situated in the area with the dominant rock process, suggesting the presence of a significant interaction between rock chemistry and water chemistry in infiltration rainwater.

a

b

Figure 10.
Gibbs diagram of the spring water samples (a: plots of TDS: Cl⁻/Cl⁻ + HCO₃₋, b: plots of TDS: Na⁺/Na⁺+Ca²⁺).

7. Saturation indices

To estimate the extent to which groundwater in the karstic aquifer could dissolve of precipitate carbonate minerals, saturation indices (SI) of calcite, dolomite, and CO_2 gas are determined to applying the samples the chemical analysis and PHREEQC software. The water was saturated due to the specified mineral if the saturation indices are zero, and water is undersaturated with mineral if it was negative; thus, the more content of mineral can be dissolved in water. When the water is supersaturated due to the specified mineral, the saturation indices will be positive. Coetsiers and Walraevens [10] represented that the more positive SI shows a higher mineral content in the water and appropriate status to precipitate in this SI. The saturation indices are provided by Eq. (1) as follows [11]:

$$SI = Log \frac{IAP}{K_t} \qquad (1)$$

where the ion activity product of the dissociated chemical species in solution with IAP is showed and the equilibrium solubility product of the chemical involved at the sample temperature with K_t is expressed [12]. The SI values due to the calcite, dolomite, and CO_2 gas determined by applying PHREEQC software are shown in **Table 3**.

Spring name	SI_c	SI_d	SI_{CO_2}
Sefidab	−0.22	−1.60	−2.49
Polahaki	0.22	−0.97	−2.16
Chopan	−0.38	−2.19	−2.10
Stakhr	0.09	−0.55	−2.22
Rajeon	0.04	−0.71	−2.02
Larneh	−0.03	−1.01	−2.28
kardemir	−0.09	−1.60	−2.60
Noor-Cheshm	−0.90	−2.88	−1.92
Sardabkhani	−0.19	−1.35	−2.09
Ghordehposhteh	−0.48	−2.09	−2.61
Kaiso	−1.60	−3.87	−2.39
Boghalamon	−0.31	−1.41	−1.36
Arbonaf	0.22	−0.31	−3.02
Naveh	−0.19	−1.34	−1.55
Kalami	−0.26	−1.75	−1.59
Spahbodan	−0.22	−1.42	−2.71
Mirhossieni	0.64	0.21	−2.16
Tochal	0.32	−0.09	−1.76
Stakhrghah	0.27	0.03	−1.89
Khani cheshme	0.62	0.67	−2.90
Rashi river	1.18	1.76	−3.23
Kaiso stream	−0.27	−0.84	−2.78
Alokale	0.27	−0.26	−1.85

Spring name	SI_c	SI_d	SI_{CO_2}
Siyavash	−0.34	−1.57	−1.54
Eshkavari	−0.12	−1.13	−1.70
Kordsara	0.76	0.71	−2.89
Bazmiyaneh	0.62	0.61	−2.62
Siyani	0.09	−0.65	−1.85
Dolisara	−1.29	−2.57	−2.35
Mina cheshme	−1.61	−3.34	−2.51

SI_c, saturation index of calcite; SI_d, saturation index of dolomite; and SI_{CO_2}, saturation index of CO_2.

Table 3.
Saturation index values of water samples (wet season).

In accordance with the saturation index values, most water samples are under-saturated due to calcite, dolomite, and CO_2 in the region; hence, carbonate minerals dissolve to a greater extent. White [13] represented that the springs with negative saturation index values (in the range from −0.2 to −0.4 or lower) have been transmitted through open conduit systems in the temperate and northern climates. A negative saturation index value of CO_2 indicates that they have no potential for travertine formation.

8. Chloro-alkaline indices

The extent to which ion occurs between groundwater and the aquifer matrix is illustrated through the chloro-alkaline indices (CAI) as suggested by Schoeller [14]. When there is an exchange between Ca and Mg in aquifer rocks with Na and K in the water (so-called "normal" ion exchange), the CAI value will be positive. When the CAI value is negative, the ion exchange is a reverse (so-called "reverse" ion exchange) [15].

The CAI value can be used as a diagnostic tool for the source of bicarbonate ion in groundwater. If the weathering of silicate minerals is the source of bicarbonate ions in water, the CAI value will have a positive amount. Conversely, if carbonate minerals were the source of the bicarbonate ions, a negative value of CAI is visible. Also, a negative CAI value shows that the source of bicarbonate can be created from human activities [16]. CAI values are calculated through Eqs. (2) and (3) as below [17]:

$$I_1 = [Cl - (Na + K)]/Cl \tag{2}$$

$$I_2 = \frac{[Cl - (Na + K)]}{So_4} + HCO_3 + Co_3 + No_3 \tag{3}$$

The CAI value of spring's water samples was calculated by Eqs. (2) and (3) (**Figure 11a** and **b**). By determining CAI value, the ion exchange in the samples and the source of bicarbonate were investigated. The results show that the four springs (t1, t2, t6, and t8) in this investigation have positive CAI values, suggesting the normal ion exchange and a bicarbonate ion source of silicate minerals. However, in other springs, the source of bicarbonate ions was carbonate minerals.
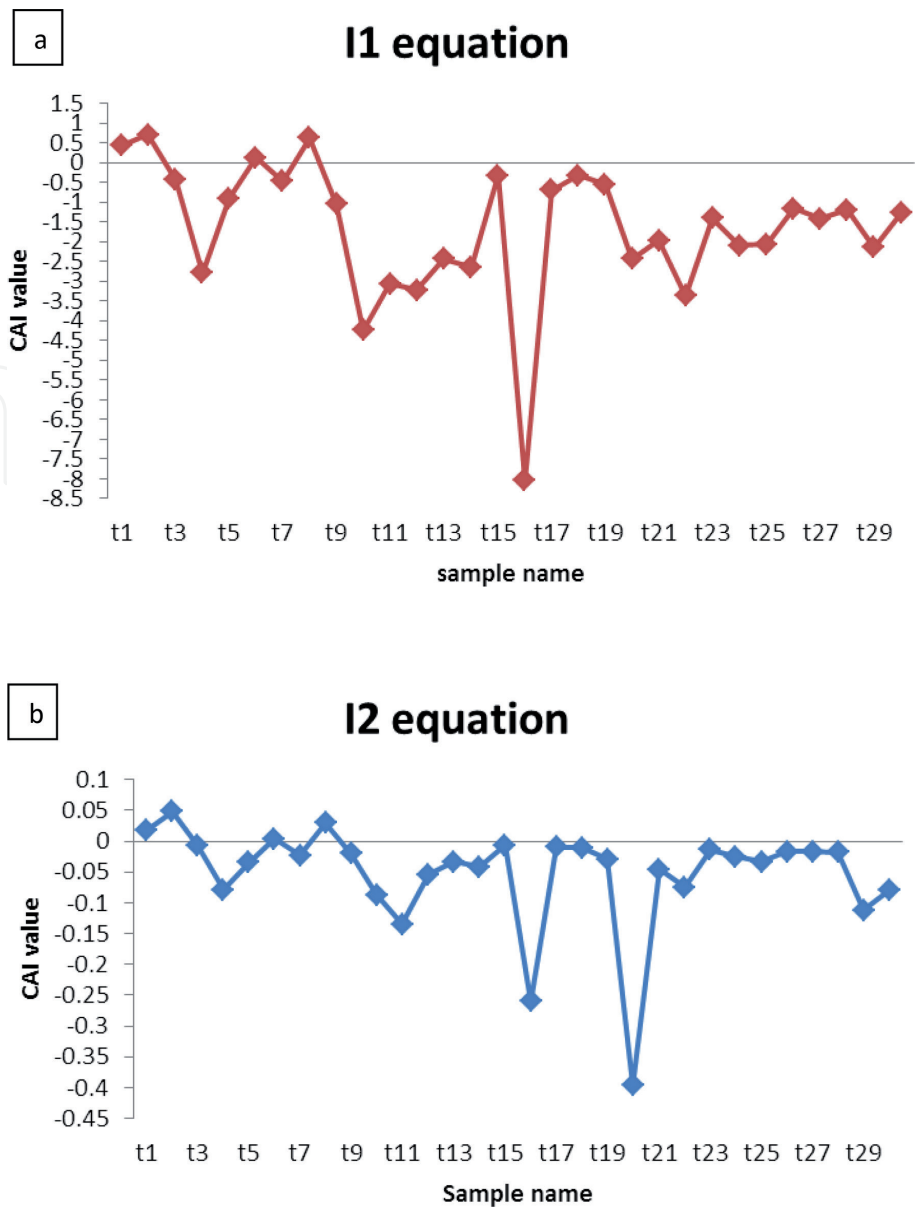
Figure 11.
The graph of chloro-alkaline index (a: relation 1 and b: relation 2).

9. Sources of ionic constituents in groundwater

By plotting the parameters of the water sample analysis on a bivariate diagram (known as a cross diagram), it is possible to interpret the processes that have impressed the chemical quality of groundwater. By plotting cations against anions, it is possible to detect the source in this method [18–22].

The common origin of the ions has been proven by the high determination coefficient between two ions. Diagrams of Ca:TDI (total dissolved ions) and Ca:HCO$_3$, and diagrams of Mg:HCO$_3$ and Mg:TDI are made to achieve this goal (**Figure 12a–d**). In order to evaluate the importance of ion exchange and different weathering process, the binary diagrams Ca + Mg:HCO$_3$ + SO$_4$ and Ca + Mg:TDI were also plotted (**Figure 12e** and **f**). If the dissolution of calcite, dolomite, and gypsum has provided Ca, Mg, HCO$_3$, and SO$_4$, there would be a 1:1 stoichiometric relationship available between Ca + Mg and HCO$_3$ + SO$_4$ [23]. The displacement of points to the right side and below the 1:1 line indicates that the ion exchange has occurred. Conversely, the displacement of points to the left side and above the 1:1 line shows the reverse ion exchange [24].
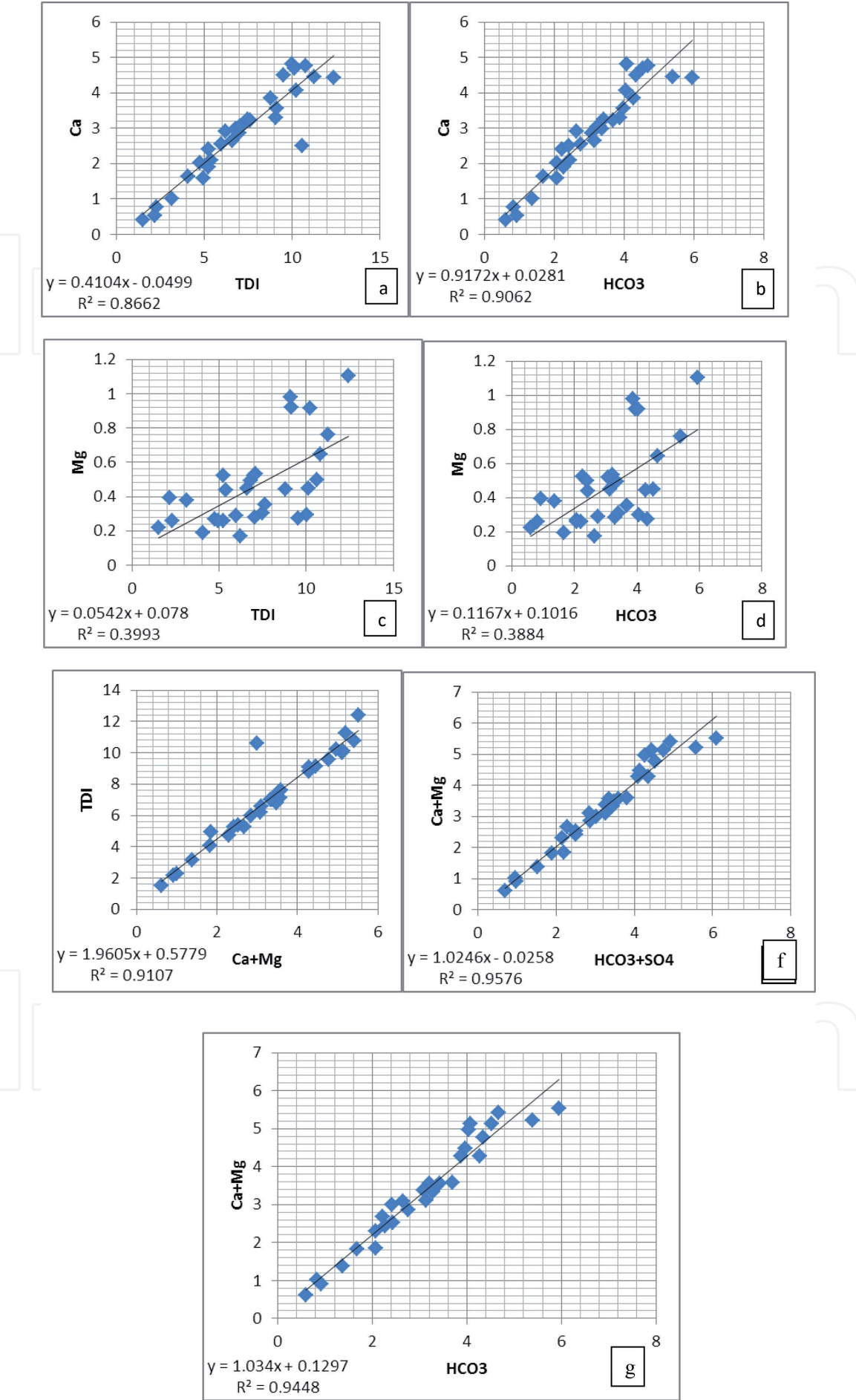
Figure 12.
Cross plot of water samples of springs (a: the plot of Ca: HCO$_3$, b: the plot of Ca: TDI, c: the plot of Mg: HCO$_3$, d: the plot of Mg: TDI, e: the plot of Ca+Mg: HCO$_3$+SO$_4$, f: the plot of Ca+Mg: TDI, g: the plot of Ca+ Mg: HCO$_3$).

Information about the stoichiometric process existence in groundwater provides the evaluation of Ca + Mg against HCO_3. The evaluation of the water quality data represents that the main source of Ca and Mg in groundwater was the dissolution of carbonate minerals, while the source of HCO_3 is likely to be the weathering of both silicate and carbonate minerals [25]. The simple dissolution was the very common weathering process for carbonates. Zhang et al. [26] presented a 1:1 ratio of Ca + Mg:HCO_3 or 1:2 molar ratio of Ca:HCO_3. As a result, through the ion exchange process of calcium and magnesium in water by the sodium in the clay, or by the cationic exchange or HCO_3 enrichment from weathering, the silicates create the low molar ratio of Ca:HCO_3 (<0.5) in groundwater [27], whereas the high ratios (>0.5) indicate the other sources of calcium and magnesium, such as reverse ion exchange, which is also created in hard rock formations with increasing salinity.

A high determination coefficient in plotting the Ca against the HCO_3 and TDI suggests that the calcium is originated from the dissolution of calcite (**Figure 12a** and **b**). Moreover, the moderate determination coefficient (classification of R^2: 0–0.3: low, 0.3–0.6: moderate, 0.6–0.9: high, and 0.9–1: very high) due to plotting the Mg against HCO_3 and TDI implies that magnesium ions may have been derived from the dissolution of dolomite (**Figure 12c** and **d**). Besides, the binary plot of Ca + Mg versus HCO_3 + SO_4 represented that 48.27% of groundwater samples shows a reverse ion exchange and 51.72% shows the ion exchange process (**Figure 12e**). The high determination coefficient due to the plotting of composite diagrams of Ca + Mg against HCO_3 indicates that these two ions have a common source, i.e., dissolution of carbonates and silicate weathering (**Figure 12g**).

10. Evaluation of the degree of karstification in recharge areas

The multiple hydrodynamic behaviors of karst aquifers were created by the development of epikarst geomorphology and the existence of sinkholes and abundant joints in limestones. Factors such as the flow hierarchy, the setting of the output, and drainage network organization in an unsaturated area have impressed the flow condition in karst systems, which are determined by the karst system structure [28]. The hydrographs of springs represent all the physical processes that have impressed groundwater flow in a karst aquifer [29]. The important method for determining the hydrological characteristics of karst aquifers is done by the analysis of hydrograph recession curves [30]. The period between peak discharge and next peak discharge at the end of the period forms the recession curve [31].

The perpetual drain of the Dorfak karst aquifer is done through the Sefidab spring, while the temporal spring is the Norcheshme spring. In the western part of the Dorfak karst area, the Sefidab spring is presented as a fault-bound spring that is situated in a fracturing zone created due to the faulting of bedded limestone. That way, the hydrograph plot was made to investigate the characteristics of the springs that include the extent of the reservoir, discharge rates, and discharge variability over time. Accordingly, the recession coefficient (α) and dynamic storage volume (as a determinant agent of aquifer development) were obtained. The discharge capacity of Sefidab spring was very variable that is related to the magnitude and duration of a precipitation event. The dynamic storage volume and recession coefficient (α) of Sefidab spring are determined through the following equations [32, 33] (**Table 4**).

$$\alpha = \frac{logQ_0 - LogQ_1}{0.4343(t)} \tag{4}$$

Coefficient	α_1	α_2	β_1	V (m³)
Sefidab spring	0.0771	0.05795	0.11331	2467838.95

Table 4.
Parameters associated with recession curve [1].

where α is the recession coefficient, Q_0 (m³/s) is a previous discharge at t = 0, Q_t (m³/s) is discharged at t, and t is the period of time between primary and secondary discharge (day).

$$V = 86400\left(\frac{Q_{01}}{\alpha_1} + \frac{Q_{02}}{\alpha_2} + \cdots + \frac{Q_{0n}}{\alpha_n}\right) \quad (5)$$

where V is the dynamic storage volume (m³), Q_{0n} is the primary discharge at n part of hydrograph plot, and α_n is the recession coefficient at n part of hydrograph plot.

The karstification degree in the recharge areas of Sefidab spring is determined through its 1-year hydrograph (due to the data loss in the monthly discharge hydrographs) and information from Malík and Vojtková [31]. Therefore, the degree of karstification of the spring is estimated to be 5.5 due to the methodology described above.

The results of the investigation are represented that Sefidab spring has a complex discharge regime, with a combination of one subregime with turbulent flow and two subregimes with the laminar groundwater flow (**Figure 13**). The impact rate of the turbulent flow subregime was short time in comparison with overall groundwater discharge. Usually, such a situation is created when there are many open medium-sized fissures (both karstified and nonkarstic) in the phreatic zone of a fissure karst aquifer (according to α_1) and with a smaller influence of connected conduits (groundwater of large karstic channels, according to β_1).

The hydrograph of Sefidab spring (the most important spring in terms of discharge) is compared with a histogram of precipitation over a 4-year period from 2011 to 2014 to investigate the precipitation effects on the karst aquifer in the study area (**Figures 14 and 15**). Three peaks can be observed in the hydrograph that the initial and tertiary peaks have occurred after two maximum rainfall events, while the second peak occurred after a period of continuous rainfall.
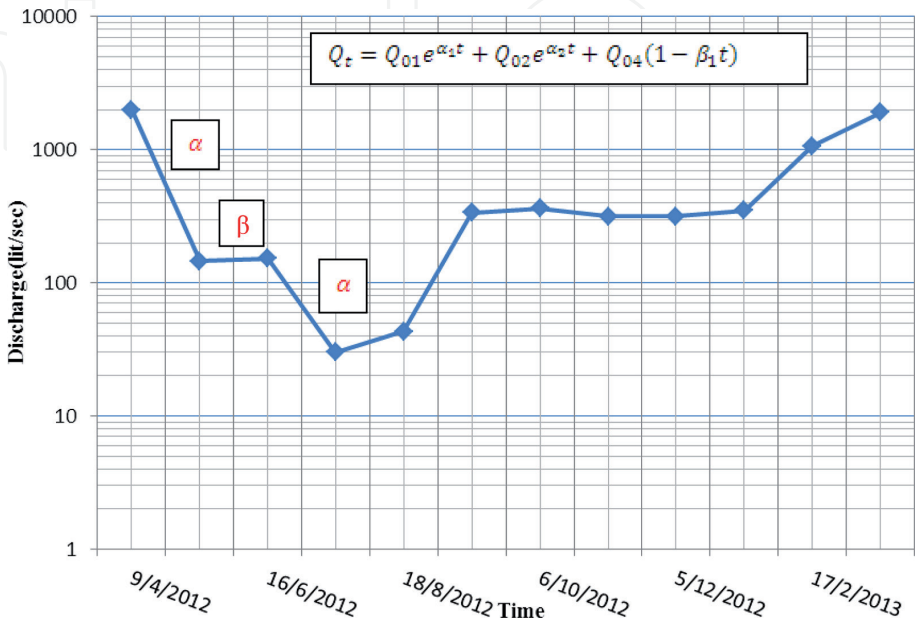

The plot shows the equation:

$$Q_t = Q_{01}e^{\alpha_1 t} + Q_{02}e^{\alpha_2 t} + Q_{04}(1 - \beta_1 t)$$

Figure 13.
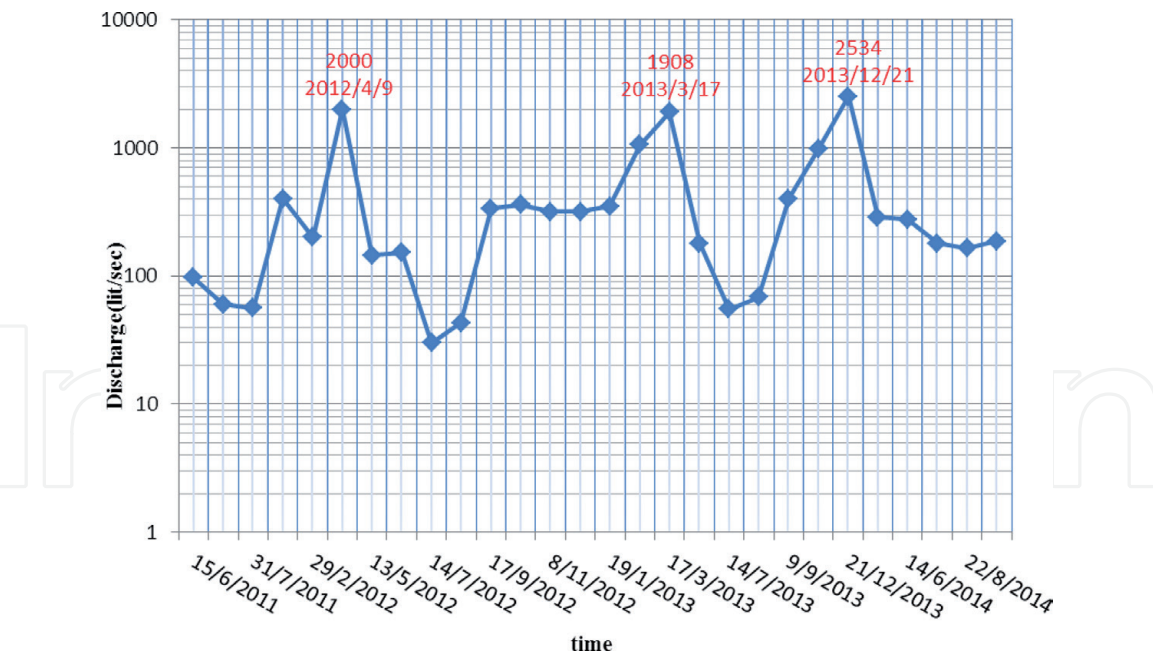*The 1-year-old hydrograph of Sefidab spring [1].*

Figure 14.
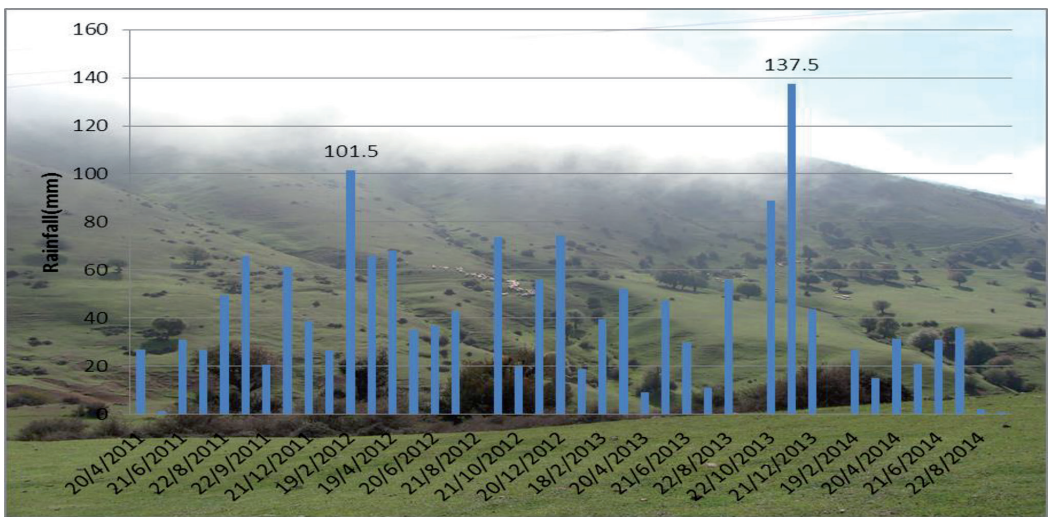*The 1-year period hydrograph of Sefidab spring [1].*

Figure 15.
The 4-year period histogram of Sefidab spring (image of Shaheshahidan pasturage) [1].

11. Chemical and microbial spring water quality

Chemical parameters and microbial agents existing on the groundwater can have a natural and human origin. The nitrate ion (NO_3) is the most important chemical parameter that shows the effect of human activity on the groundwater quality. The nitrate ion in the groundwater originates from urban wastewater influx, industrial, fertilizer, and animal excreta. Based on our measurements, the highest value of the nitrate ion was 1.392 meq/l for Soltankhani spring that is higher for world hygiene organization's limit. The high nitrate value was due to the occurrence of some cottage and pasture in the upstream of the Soltankhani spring due to the animal and human excreta influx. Except for the Soltankhani spring, all appointive samples of the nitrate values have a favorable value in both wet and dry seasons. The water microbial contamination is usually determined based on the number and frequency of the special type of bacteria. The coliforms are the dominant index of microbial quality of the water resource that is frequently found in the human excreta and

other endotherm animals. The most prevalent bacteria in the coliform group are *Escherichia coli* that are excreta contamination index of the water. The microbial contamination can be observed in all samples due to the intense development of karst, lack of self-purification in the karst system, and lack of an adequate cover layer on carbonate formation. Although the major elective samples have the better status of microbial contamination in the wet season than the dry season, the accomplishment of sanitary preparation and infiltration before consumption (among boiling of water and surcharge of chlorine) is of great necessity.

12. Contamination hazards in the spring catchment and vulnerability mapping

Potential hazards to the karst aquifer were created mainly from forestry, pasture, tourism, and an unnaturally high game population (mainly, chamois and deer) except airborne pollution. The input from tourism, pasture, and the game population was mainly feces with their microbial contaminations [34]. Karst systems with joints and clefts and without a self-purification inexistence pose a high vulnerability to human activities. The high hydraulic conductivity, transmissivity, and intense heterogeneity and anisotropy of karst aquifers enhance their vulnerability to dopants. Various methods can be applied to the vulnerability analysis of karst aquifers. Kardan Moghadam et al. [35] applied the EPIK vulnerability index that consists of four parameters: epikarst, the preservative cover layer, permeation condition, and developed karst system. Preparation, weighing operation, and incorporation of the suitable parameters map was accomplished in the ArcGIS environment [35]. The Dorfak peak Polje can enhance the vulnerability level of karst aquifer due to livestock aggregation in the spring and summer seasons. The risk map is provided through incorporating this information with vulnerability index [35]. In general, carbonates in the study area were very well karstified throughout and covering layers were mostly absent, not protective, and sometimes even increased the point recharge. Vulnerability, according to the EPIK method (**Figure 16**), is high in 20% of the area (20% high vulnerability, 35% moderate vulnerabilities, and 45% low vulnerabilities) [35].
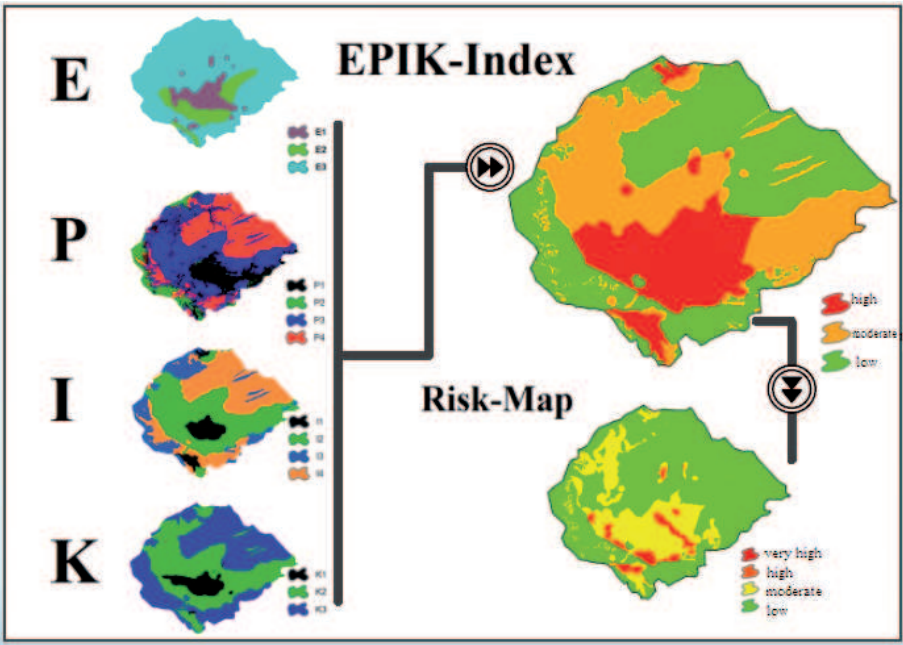

Figure 16.
Risk map of the study area (reproduced with the permission from Kardan Moghadam et al. [35]).

Acknowledgements

Glossary

m.a.s.l:	abbreviation of meters above sea level, elevation
Csa:	hot dry-summer" Mediterranean climates
Bsk:	cold semiarid Mediterranean climates
TDS (total dissolved solids):	it is a measurement of the soluble composed of amount of all organic and inorganic materials existing in a liquid in a microgranular (colloidal sol) suspended form, ionized or molecular.
Karren:	these are channels or furrows that were created due to dis solution on massive bare limestone surfaces; their depth changes from a few millimeters to more than a meter and is discredited by ridges.
Shaft:	it is a cylindrical tube commonly steep-sided, which is created due to dissolution and (or) collapse.
Polje:	it is a Slavic word for field. They are a very large closed depression in areas of karst topography; their length and width vary by several kilometers in some places, having a flat floor, both covered by alluvium or bare Limestone, and blockaded generally by steep walls of limestone.
Grike:	these are vertical or subvertical fissures in a limestone pavement that are created through solution along with a joint. Their synonym is Kluftkarren (in the German language).
Clint:	these are slabs of limestone, parallel to the bedding, forming a pavement. Widened joints, or grikes, are isolated individual clints. The synonym term is Flachkarren.
Kamenitzas:	the form of the kamenitzas (solution pans) looks like a dish or a plate.
Rinnenkarren:	these are the solution grooves named in the German language and are created where the runoff water has gathered in streams. If the total surface is wetted, the content of water increases downward, and in this case, the grooves were broadened and deepened at their bottom.
Meandering runnel:	their cross section were asymmetrical. They are sometimes meandering and are frequently created as isolated features on gentle slopes (less than 10°).
Wall karren:	these are formed on vertical walls as a result of water flowing down the walls without any wide-spreading moistening although wide-spreading wet down ing occasionally impresses their development.
Hummocky karren:	these are constructed due to bulge and depression created by solution on the rock surface.
Trittkarren:	these are best characterized as heel-print karren because they look like the imprint of a heel. They are linked nearly with subhorizontal, adjacent, flat plains, and immigrated upslope by cutting "steps" through the process of retrogres sive corrosion.

Rainpit:	their depth and diameter vary by several centimeters. The shape of the rainpit is circular (from above) and spherical calotte (in lateral view). According to Jennings (1985), they are formed by raindrops (e.g., falling from leaves).
Rillenkarren:	these occur only in places where fresh unspent precipitation is active and end where the water attains too high a content of lime or where water is added.
Rundkarren:	these are solution channels or furrows, which are developed beneath a soil cover.
Cavernous karren:	these are pitted, rubbly limestone most commonly found in relatively recent and tertiary limestones of the humid tropics.

Author details

Maryam Dehban Avan Stakhri[1*], Mohammad Hossien Ghobadi[2] and Ali Mirarabi[3]

1 Engineering Geology, Faculty of Sciences, Bu-Ali Sina University, Hamedan, Iran

2 Department of Geology, Faculty of Sciences, Bu-Ali Sina University, Hamedan, Iran

3 Hydrogeology, Faculty of Sciences, Shahid Beheshti, Tehran, Iran

*Address all correspondence to: mdehban84@gmail.com

IntechOpen

References

[1] Ghobadi MH, Dehban Avan Stakhri M, Mirarabi A. Investigating the hydrogeological properties of springs in a karstic aquifer in Dorfak region (Guilan Province, Iran). Environmental Earth Sciences. 2018;**77**:96. DOI: 10.1007/s12665-018-7270-4

[2] Safari HO, Ghassemi MR, Razavi-Pash R. Determination and structural analysis of the Lahijan transverse fault in forestall region of Alborz mountains, Iran: A geospatial application. International Journal of Remote Sensing Applications. 2013;**3**(4):215-224. DOI: 10.14355/ijrsa.2013.0304.06215

[3] Piper AM. A graphic procedure in the geochemical interpretation of water analyses. American Geophysical Union, Transactions. 1944;**25**:914-923

[4] Singhal BBS, Gupta RP. Applied Hydrogeology of Fractured Rocks. Kluwer Academic Publisher; 1999. p. 400

[5] Giggenbach WF. Geothermal solute equilibria. Derivation of Na–K–Mg–Ca geoindicators. Geochimica et Cosmochimica Acta. 1988;**52**:2749-276

[6] Mirarabi A. The identification of Dorfak karstic regions, Divrash and Shahr-e-Bijar watersheds. Report of Regional Water Company of Guilan Province. 2015 (in Persian)

[7] Subba Rao N. Geochemistry of groundwater in parts of Guntur district, Andhra Pradesh, India. Environmental Geology. 2002;**41**:552-562

[8] Gibbs RJ. Mechanism controlling world water chemistry. Science. 1970;**170**:1088-1090

[9] Li PY, Qian H, Wu JH, Ding J. Geochemical modeling of groundwater in southern plain area of Pengyang County, Ningxia, China. Water Science and Engineering. 2010;**3**(3):282-291

[10] Coetsiers M, Walraevens K. Chemical characterization of the Neogene Aquifer, Belgium. Hydrogeology Journal. 2006;**14**:1556-1568

[11] Garrels R, Mackenzie F. Origin of the chemical compositions of some springs and lakes. In: Ground RF, editor. Equilibrium Concepts in Natural Water Systems. Washington: American Chemical Society Publications; 1967

[12] Singh EJ, Gupta A, Singh NR. Groundwater quality in Imphal West district, Manipur, India, with multivariate statistical analysis of data. Environmental Science and Pollution Research International. 2013;**20**:2421-2434

[13] White WB. Thermodynamic equilibrium, kinetics, activation barriers, and reaction mechanisms for chemical reactions in karst terrains. Environmental Geology. 1997;**30**:46-58

[14] Schoeller H. Geochemistry of groundwater. In: Groundwater Studies—An International Guide for Research and Practice. Vol. 15. Paris: UNESCO; 1977. pp. 1-18

[15] Aghazadeh N, Asghari Moghaddam A. Investigation of hydrochemical characteristics of groundwater in the Harzandat aquifer, Iran. Environmental Monitoring and Assessment. 2011;**176**:183-195

[16] Chidambaram S, Karmegam U, Prasanna MV, Sasidhar P, Vasanthavigar M. A study on hydrochemical elucidation of coastal groundwater in and around Kalpakkam region, Southern India. Environmental Earth Sciences. 2011;**64**:1419-1431

[17] Schoeller H. Geochemistry of Groundwater: An International Guide for Research and Practice Book. India: UNESCO; 1965. pp. 1-18

[18] Howard FWK, Mullings E. Hydrochemical analysis of groundwater flow and saline intrusion in the Clarendon basin, Jamaica. Groundwater. 1996;**34**:801-810

[19] Stossel RK. Delineating the chemical composition of the salinity source for saline groundwater: An example from east central Canadian Parish, Louisiana. Ground Water. 1997;**35**:409-417

[20] Stober I, Bucher K. Deep groundwater in the crystalline basement of the Black Forest region. Applied Geochemistry. 1999;**14**:237-254

[21] Timms W, Acworth RI, Jankowski J, Lawson S. Groundwater Quality Trends related to Aquitard Salt Storage at Selected Sites in the Lower *Murumbidgee alluvium*, Australia. Groundwater. 2000;**25**:655-660

[22] Marie A, Vengosh A. Sources of salinity in groundwater from Jericho area, Jordan Valley. Ground Water. 2001;**39**:240-248

[23] McLean W, Jankowski J, Lavitt N. Groundwater quality and sustainability in an alluvial aquifer, Australia. In: Sililo O et al., editors. Groundwater, Past Achievements and Future Challenges. Rotterdam: A Balkema; 2000. pp. 567-573

[24] Krishnaraj S, Murugesan V, Vijayaraghavan K, Sabarathinam C, Paluchamy A, Ramachandran M. Use of hydrochemistry and stable isotopes as tools for groundwater evolution and contamination investigations. Geosciences. 2011;**1**(1):16-25. DOI: 10.5923/j.geo.20110101.02

[25] Srinivasamoorthy K, Vasanthavigar M, Vijayaraghavan K, Sarathidasan R, Gopinath S. Hydrochemistry of groundwater in a coastal region of Cuddalore district, Tamilnadu, India: Implication for quality assessment.

Arabian Journal of Geosciences. 2011. DOI: 10.1007/s12517-011-0351-2

[26] Zhang J, Huang WW, Letolle R, Jusserand C. Major element chemistry of the Huanghe (Yellow River), China—Weathering processes and chemical fluxes. Journal of Hydrology. 1995;**168**:173-203

[27] Drever JI. The Geochemistry of Natural Waters. 3rd ed. New Jersey: Prentice Hall; 1997. p. 436

[28] Lastennet R, Mudry J. Role of karstification and rainfall in the behavior of a heterogeneous karst system. Environmental Geology. 1997;**32**(2):114-123

[29] Kuhta M, Brkić Ž, Stroj A. Hydrodynamic characteristics of Mt. Biokovo foothill springs in Croatia. Geologia Croatica. 2012;**65**(1):41-52

[30] Kresic N, Bonacci. Spring discharge hydrograph. In: Groundwater Hydrology of Springs: Engineering, Theory, Management, and Sustainability. Elsevier; 2010. pp. 129-163. Ch. 4

[31] Malík P, Vojtková S. Use of recession-curve analysis for estimation of karstification degree and its application in assessing overflow/underflow conditions in closely spaced karstic springs. Environmental Earth Sciences. 2012;**65**(8):2245-2257

[32] Castany G. Prospection et Exploitation des Eaux Souterraines. Paris: DUNOT; 1968

[33] Mijatovic B. A Method of Studying the Hydrodynamic Regime of Karst Aquifers by Analysis of the Discharge Curve and Level Fluctuation During Recession. Beograd: Institute for Geological and Geophysical Research; 1970

[34] Plan L, Kuschnig G, Stadler H. Kläffer Spring—The major spring of

the Vienna water supply (Austria). In: Kresic N, Stevanovic Z, editors. Groundwater Hydrology of Springs. Butterworth-Heinemann: Elsevier; 2010. pp. 592-411. DOI: 10.1016/C2009-0-19145-6

[35] Kardan-Moghadam H, Javadi S, Kavosi-Hydari A, Mirarabi A. Evaluation of Dorfak Karst Aquifer intrinsic vulnerability with EPIK method in the North of Iran. In: First International Conference on Water Environment and Sustainable Development; 27-29 September 2016; Ardabil, Iran. 2016. in Persian